Computational Methods in CONTACT MECHANICS IV

Editors: L. Gaul and C.A. Brebbia

WIT PRESS

Computational Methods in Contact Mechanics IV

EDITORS:

L. Gaul
University of Stuttgart, Germany

C.A. Brebbia
Wessex Institute of Technology, UK

WITPRESS Southampton, Boston

Studies into contact interactions of elastic bodies for improvement of wheels and rails

V. Yessaulov[1], A. Kozlovsky[2], Y. Taran[1] and A. Sladkovsky[2]
[1]State Metallurgical Academy, Prospekt Gagarina, 4, Dnepropetrovsk, 320635, Ukraine
Email: dmeti@dmeti.dnepropetrovsk.ua
[2]JSC Nizhnedneprovsk Tube-Rolling Plant

Abstract

A two-zone microslip theory was used to study cylinder rolling contact. The theory was validated by experiment. The experimental study involved direct strain-gage measurements in the contact area of the rolling cylinders. The state of strain in the wheel/rail contact region was studied. Contact region stress distributions for various relative positions of the wheelset with respect to the rail track were determined. Angles of attack were accounted for. The computational results were used to design improved contours of wheel tread and rail head.

1 Introduction

A study into wheel/rail contact interaction should include an analysis of the state of stress at the wheel and rail running surfaces in the vicinity of the contact region. Microslip is known to influence the distribution of the adhesion zone and the relative slip region at the interacting surfaces and, consequently, the profiles of contact stresses and the surface wear. A study into the microslip effect is therefore mandatory for understanding the state of stress in interacting bodies. As is well-known, there are several theories concerning the number of adhesion zones and slip zones in contact interaction. For cylinders with identical elastic constants, the two-zone theory put forward by F.W. Carter and H. Fromm is more widely accepted. According to this theory, the adhesion zone adjoins the contact region entry while the slip zone is near the exit. Furthermore, as the tractive force is increased, the slip zone is expanded at the

expense of the adhesion zone. There are solutions for other theories; for example, H. Poritsky considered a similar contact problem involving three zones, namely a middle adhesion zone and two slip zones. Therefore, a three-dimensional contact problem of wheel/rail interaction can be solved using the band theory, provided that reliable information is available on the distribution of the adhesion and slip zones for two rolling cylinders or a cylinder rolling on a plane.

However, when two contact regions exist in the wheel/rail system, the contact problem becomes more complex, especially at nonzero angles of attack. Importantly, it is in this case that the wear rate in the flange zone is at a maximum as a result of slip occurring here. A study into wheel/rail contact interactions may suggest changes in the running surface contours with a view to extending running surface lives.

2 Microslip in rolling cylinders

Several researchers studied microslip using strain gages. A common limitation of those studies was that the strain gages were embedded in the contacting bodies at depths comparable to or greater than the contact region width. The strain gage spans also were fairly long. It is therefore desirable to determine the limiting depth and optimum orientation for a short-span strain gage to be able to pinpoint the microslip zones.

Consider rolling contact of two elastic cylinders with the radii of R_1 and R_2, forced against each other by the force P and capable of transmitting a tractive force T. Let the Y-axis go through the centers of the cylinders and the X-axis be aligned with the contact region. A complex analysis of the state of stress and strain in the vicinity of cylinder contact region revealed that the effects of microslip are most pronounced in the distribution of strains γ_{xy} measured by strain gages inclined to the X-axis at an angle of 45°. The plot features associated with the microslip can be traced down to a depth of $0.7b$, where b is the contact region halfwidth. Clearly, the experimental research should involve cylindrical models whose moduli of elasticity must be at least one order of magnitude below that of actual wheels. Furthermore, there are two ways to increase the contact region width. The first way is to increase P but it is narrowly limited by the characteristics of the experimental setup and the necessity to avoid plastic deformations in the test cylinders. The second way is to increase the diameters of the model cylinders. A test unit was designed that precluded misalignments in loading and ensured the desired contact interaction conditions. The cylinder diameter could be as high as 0.5 m, and the contact region width could thus be increased to 12 mm.

The deformations at wheel sides were measured using foil- and wire-type strain gages with a span of 1 mm. Some of the measured deformation profiles exhibited microslip. However, a reliable estimate of the number of microslip zones is only possible at strain gage depths equal to or less than $0.03b$. It is

difficult to provide such shallow positions of strain gages at wheel sides or inside a wheel. For this reason, a technique was developed that involved bonding strain gages directly to the running surfaces of test cylinders made of a special rubber with a modulus of elasticity equal to 9.44 MPa. The stress-strain curve of the rubber was such that it could be considered a linear elastic material at loads up to 0.2 MPa.

Figure 1 depicts ε_{xx} strain profiles for the contact surface of a driven cylinder at various values of the tractive force T. The figure gives three wheel rolling plots constructed for one value of the vertical force P and three different values of the tractive force $T = M/R$, M being the torque applied to wheel axis, R the wheel radius. Each plot corresponds to one or other of the tractive force values T_i ($T_1 > T_2 > T_3$). The direction of rolling is determined by the angular speed ω. Within the contact region $[-b,b]$ the plots exhibit two sections, namely $[\alpha_i,b]$ with nearly parabolic distributions and $[-b,\alpha_i]$ where the strains decrease until any contact disappears at $x=-b$. The points α_i thus mark the boundary between the slip zone and the adhesion zone.

This conclusion is supported by comparison of the experimental data with a theoretical solution based on Glagolev's results [1].

The strain distribution in the contact region can be obtained using functions $\Phi(z)$ and $\overline{\Phi}(z)$ of a complex variable $z = x + iy$. Applying the aforementioned solution [1], one can write

$$\Phi(z) = \frac{\mu f i}{R(\chi+1)}\left[\left(1+\frac{2}{fi}\right)\sqrt{b^2-z^2} - \sqrt{(z-\alpha)(b-z)} + \frac{i(b+\alpha)}{2}\right] \quad (1)$$

$$\overline{\Phi}(z) = \frac{\mu f i}{R(\chi+1)}\left[\left(1-\frac{2}{fi}\right)\sqrt{b^2-z^2} - \sqrt{(z-\alpha)(b-z)} + \frac{i(b+\alpha)}{2}\right] \quad (2)$$

$$R = \frac{R_1 R_2}{R_1 + R_2}, \qquad \chi = \frac{\lambda + 3\mu}{\lambda + \mu} \quad (3)$$

where R_1, R_2 are the wheels radii, λ and μ the Lamu constants, f the coefficient of friction. The contact region halfwidth is

$$b = \sqrt{\frac{P(\chi+1)R}{\pi\mu}} \quad (4)$$

The boundary α is defined as

$$\alpha = b - 2b\sqrt{1-\frac{M}{fPR}} \quad (5)$$

where M is the torque applied to the wheel axis. Using Muskhelishvili's relationships [2], one finds for the derivative of wheel displacements u along the X-axis

$$4\mu u^{+'}(z) = -\chi\left(\Phi^{+} + \overline{\Phi}^{-}\right) - \Phi^{-} - \overline{\Phi}^{+} \tag{6}$$

Making allowance for nonuniqueness of the solutions, one obtains through substitution of Eqs. (1) and (2) to (6) and subsequent passage to the limit at a contact plane for the strain ε_{xx} =

$$= \begin{cases} \dfrac{f(b+\alpha)}{4R} - \dfrac{f}{2R}\sqrt{(\alpha-x)(b-x)} + \dfrac{f}{2R}\sqrt{x^2-b^2} & , \quad -\infty < x \le -b \\ \dfrac{f(b+\alpha)}{4R} - \dfrac{f}{2R}\sqrt{(\alpha-x)(b-x)} - \dfrac{\chi-1}{R(\chi+1)}\sqrt{b^2-x^2} & , \quad -b \le x \le \alpha \\ \dfrac{f(b+\alpha)}{4R} - \dfrac{\chi-1}{R(\chi+1)}\sqrt{b^2-x^2} & , \quad \alpha \le x \le b \\ \dfrac{f(b+\alpha)}{4R} + \dfrac{f}{2R}\sqrt{(\alpha-x)(b-x)} - \dfrac{f}{2R}\sqrt{x^2-b^2} & , \quad b \le x < \infty \end{cases} \tag{7}$$

These equations have to do with the driven wheel. Substitution of $-M$ and $-F$ for M and F respectively in each equation results in similar relationships for the driving wheel.

A strain gage measures average strains along its span. Therefore, a theoretical profile of the strain ε must be determined and compared with experimental data:

$$\varepsilon = \frac{1}{l}\int_{c_2}^{c_1} \varepsilon_{xx}(x)\,dx \tag{8}$$

Here, the integration is effected with respect to x along the span l of a "mathematical" strain gage between the limits $c_2 = x_c - l/2$ and $c_1 = x_c + l/2$, x_c being the center of the strain gage. Following relationships are thus derived

$$\varepsilon = \begin{cases} S_1 - S_2 + S_3 & , \quad -\infty < x \le -b \\ S_1 - S_2 - S_4 & , \quad -b \le x \le \alpha \\ S_1 - S_4 & , \quad \alpha \le x \le b \\ S_1 + S_2 - S_3 & , \quad b \le x < \infty \end{cases} \tag{9}$$

where the functions $S_i(c_1, c_2)$ are eventually dependent on the strain gage coordinate x_c and defined as follows

$$S_1 = \frac{f(b+\alpha)}{4R} \tag{10}$$

$$S_2 = \frac{f}{16R(c_1-c_2)}\Big[2(2c_1-\alpha-b)\sqrt{(\alpha-c_1)(b-c_1)} -$$

$$-2(2c_2-\alpha-b)\sqrt{(\alpha-c_2)(b-c_2)}+(4\alpha b-$$

$$-(\alpha+b)^2)\ln\frac{2\sqrt{(\alpha-c_1)(b-c_1)}+2c_1-\alpha-b}{2\sqrt{(\alpha-c_2)(b-c_2)}+2c_2-\alpha-b}\Bigg] \tag{11}$$

$$S_3=\frac{f}{4R(c_1-c_2)}\Bigg[c_1\sqrt{c_1^2-b^2}-c_2\sqrt{c_2^2-b^2}-$$

$$-b^2\ln\frac{\sqrt{c_1^2-b^2}+c_1}{\sqrt{c_2^2-b^2}+c_2}\Bigg] \tag{12}$$

$$S_4=\frac{\chi-1}{2R(\chi+1)(c_1-c_2)}\Bigg[c_1\sqrt{b^2-c_1^2}-c_2\sqrt{b^2-c_2^2}+$$

$$+b^2\arcsin\frac{c_1}{b}-b^2\arcsin\frac{c_2}{b} \tag{13}$$

Equations (9) through (13) were used for comparison between the theoretical and experimental strain profiles. Almost complete qualitative agreement between theory and experiment was observed, so no theoretical profiles are shown. The only exception was the zone ahead of the contact region entry. The experiment revealed a small wave in this zone as shown in Fig. 1 but no such zone was present in the theoretical profiles. The quantitative values of theoretical plots are more than two times as great as the experimental data. This is a result of the strain gage stiffness being comparable to that of the wheel material. A strain gage this stiffens the low-modulus material used in the experiments. A finite element technique combining theory and experiment was used to determine the stiffening factor [3] employed to make necessary corrections. The quantitative comparison of the resulting plots demonstrated their good agreement, leading to a conclusion that for rolling contact between two wheels with similar elastic constants the two-zone theory of microslip is acceptable. Similar plots were constructed for the driving wheel, Fig. 2. In the absence of a tractive force (torque) the entire contact region is evidently occupied by the adhesion zone, both in the case of two cylinders and a cylinder rolling on an infinite half-space. As the tractive force is increased to its critical value $T = fP$, the appearing slip zone grows at the expense of the adhesion zone to the point of breakdown associated with slippage. The microslip was studied for a better understanding of wheel/rail contact interaction. The geometric slip or creepage, however, is responsible for a much greater contribution to the overall wear of wheel flanges.

3. Wheel/rail contact interaction

When the wheel flange is forced against the rail side, the contact between the wheel and the rail takes place in two regions; such are the cases of rolling in curves or wheelset hunting on straight track. Since the local wheel radii in the two contact regions are different, complete slippage occurs in one of the regions. This is schematically represented in Fig. 3 for the angle of attack ζ. The flange contact region B then leads the prime contact region A, the advance being denoted as a. A major factor affecting wear of wheel flanges and rail sides is the lateral guiding force Q transmitted from the rail to the wheel flange in region B. This force is at a maximum in running in curves when the angle of attack attains a maximum. Normally it happens when the vehicle runs to a side track. In this case

$$\zeta = \frac{2\Delta}{L} + \sqrt[3]{\frac{9\Delta^2}{4C}} \tag{14}$$

where 2Δ is the maximum gap between the wheel flange and the rail side, L the vehicle base, C the transition curve parameter. The angle of attack also is a function of the wheel gap in the new wheelset, the values of wheel wear in the wheelset, elastic deformations in the wheel axle box etc. The advance a of region B with respect to the instantaneous axis of wheel rotation is normally governed [4] by

$$a = (r + \tau)\tan\zeta\tan\tau \tag{15}$$

where r is the wheel radius, t the distance between the uppermost level of the rail head and the flange contact point in region B, τ the angle of the flange rolling surface inclination to horizontal. Clearly, finding a for a curvilinear tread contour, especially of a worn wheel, is a fairly complex mathematical problem. Yet it is the advance that determines the location of contact region B and therefore the values of the guiding force and of the flange wear which is a function of the energy A dissipated through friction in region B when the wheel turns by an angle γ with respect to its instantaneous axis,

$$A = fQa\gamma\cos\zeta \tag{16}$$

Mathematically, a problem of running surface contour design for wheels and rails can thus consist in minimization of the functional A, because at given values of the angle of attack ζ and the angle of wheel rotation γ which normally is taken equal to 1, A is a function of Q and a which are determined by a number of considerations, the major one being the geometry of the wheel and the rail interacting with each other.

Consider the statement of problem of pinpointing contact regions A and B for nonzero angles of attack. The Z-axis is assumed to be directed along the lane. The rail running surface contours are given by

$$y = f_i(x) \quad , \qquad y = f_e(x) \quad , \qquad -\infty < z < \infty \tag{17}$$

describing noncircular cylindrical surfaces for the inner and the outer rail respectively. Being relatively large, the track curve radius is not taken into

account. The Eqs. (17) account for the cant of the rails and the actual track gage, including side wear and elastic displacements of the rails.

A wheel tread can be described as follows. For the outer wheel and a middle position of the wheelset with respect to the lane, the surface can be represented in a parametric form

$$\begin{aligned} X &= x_w \\ Y &= r_m - \left[r_m - y_w(x_w)\right]\cos\varphi \\ Z &= \left[r_m - y_w(x_w)\right]\sin\varphi \end{aligned} \tag{18}$$

where the first parameter x_w is the abscissa of the contour generating line in a system of coordinates associated with the tread contour (Fig. 3), y_w the function describing the wheel running surface contour that generally can be given in a numerical form, r_m the maximum radius at the flange, φ the second parameter, namely the wheel central angle. When a wheelset undergoes a displacement δ across the lane and turns by an angle ζ in rolling, the second relationship in (18) remains unchanged while the first and the third one have to be rewritten as

$$X = (x_w + \delta)\cos\zeta + \left[r_m - y_w(x_w)\right]\sin\varphi\sin\zeta \tag{19}$$

$$Z = -(x_w + \delta)\sin\zeta + \left[r_m - y_w(x_w)\right]\sin\varphi\cos\zeta \tag{20}$$

These relationships constitute a parametric representation of the wheel surface that contacts the rail surface described by (17). The task of mathematical treatment now consists in finding the vertical distance or the height h of point $W(X,Y,Z)$ belonging to the tread, with respect to the rail surface. Clearly, h is a function of tread parameters, that is $h = h(x_w, \varphi)$. It is necessary to minimize h over the set of allowable values for any x_w and φ. In the case of the function A having a single minimum, its corresponding parameter values x_w and φ define the tread point which is the initial point of contact with the rail running surface. When there are two minima, we probably have to deal with a case of two contact regions. An algorithm of search for regions A and B was described earlier [5]. It can also be utilized for finding contact stress distributions in the two regions.

The above theoretical and experimental approaches were employed for designing new contours of wheel and rail running surfaces. The tread contours developed for railroad cars and locomotives are purely curvilinear and were named DMetI profiles after the Dnepropetrovsk Metallurgical Institute, now State Metallurgical Academy of Ukraine. Among other things, the present writers described wheel/rail interactions for standard wheels to GOST 9036-88 and R65 rails used in the former USSR [5]. For the case at hand, the interaction in region B is accompanied by calculated frictional losses of energy A = 38.1 J.

The same analysis yielded a value of A = 4.14 J for DMetI LB wheel profile. The maximum contact stresses in region B of wheels with newly developed profiles were found to be decreased by 25 to 30 %. This results in lower plastic deformation of wheel material in the flange region. Fig. 4 depicts some computer simulation data on DMetI LB wheel/R65 rail contact. Here, σ_1 and σ_2 are the maximum stresses in the regions B and A respectively. The new profiles reduced wear and extended wheel life in actual service.

Similar research was conducted for rails, resulting in development of rails with asymmetrical head contour. The rails are currently being tested under actual service conditions. In in-plant line service they exhibited a 50% extension in life compared to the standard R65 rails at sections with heavy traffic loads. The underlying methodologies can be employed for designing wheels and rails intended for various axle forces, running speeds and other service parameters.

References

1. Glagolev, N.I., Friction and wear in rolling of cylindrical bodies, *Inzhenernyi Zhurnal AN SSSR*, 1964, **4**, 659-672. In Russian.
2. Muskhelishvili, N.I., *Some principal problems of mathematical theory of elasticity*, Nauka Publishing House, Moscow, 1966. In Russian.
3. Petrov, V.V. & Sladkovsky, A.V., The factor of stiffening of low-modulus materials by strain gages, *Metrologiya*, 1986, **6**, 54-60. In Russian.
4. Verigo, M.F. & Kogan, A.Ya., *Interactions between rolling stock and railroad track*, Transport Publishing House, Moscow, 1986. In Russian.
5. Yessaulov, V., Taran, Y., Sladkovsky, A., Kozlovsky, A. & Shmurygin N. Design of wagon wheels using the finite element method, *Computers in Railways V*, Vol.2, pp 69-77, Computational Mechanics Publications, Southampton & Boston, 1996.

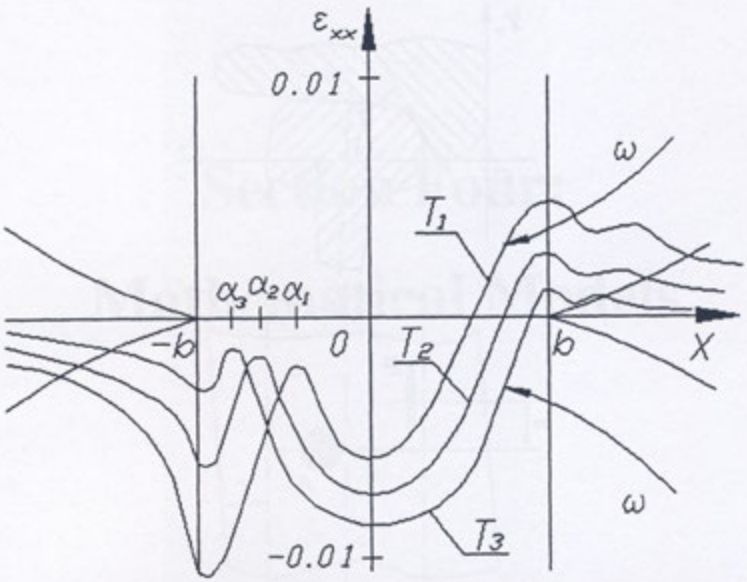

Figure 1. ε_{xx} surface strain profiles for a driven cylinder at various tractive forces $T_i (T_1 > T_2 > T_3)$

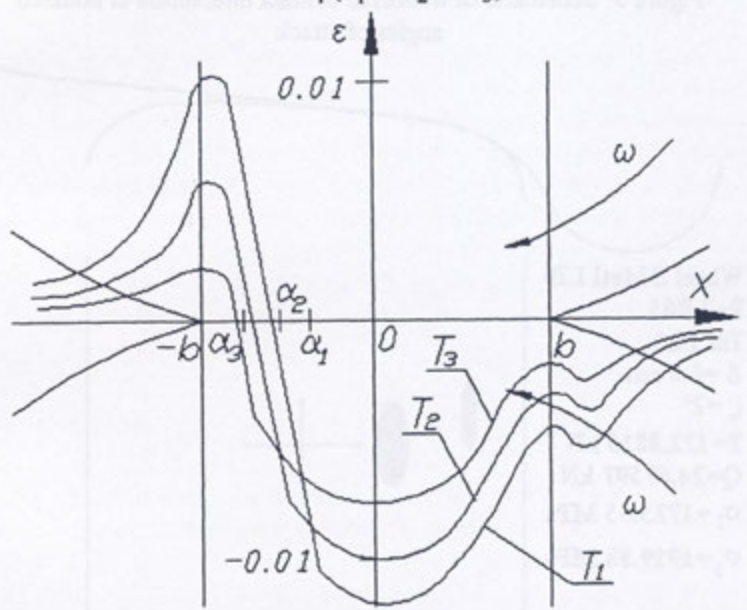

Figure 2. ε_{xx} surface strain profiles for a driving cylinder at various tractive forces $T_i (T_1 > T_2 > T_3)$

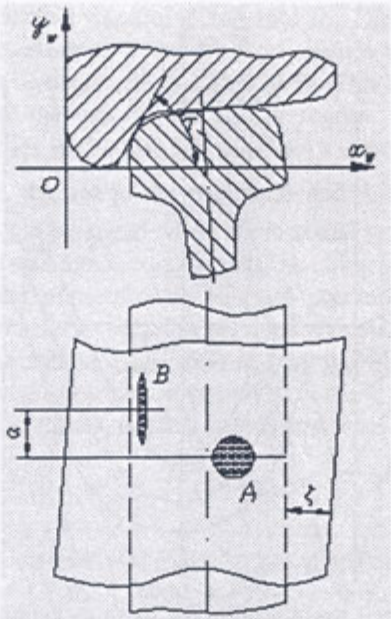

Figure 3. Schematic of wheel/rail contact interaction at nonzero angles of attack

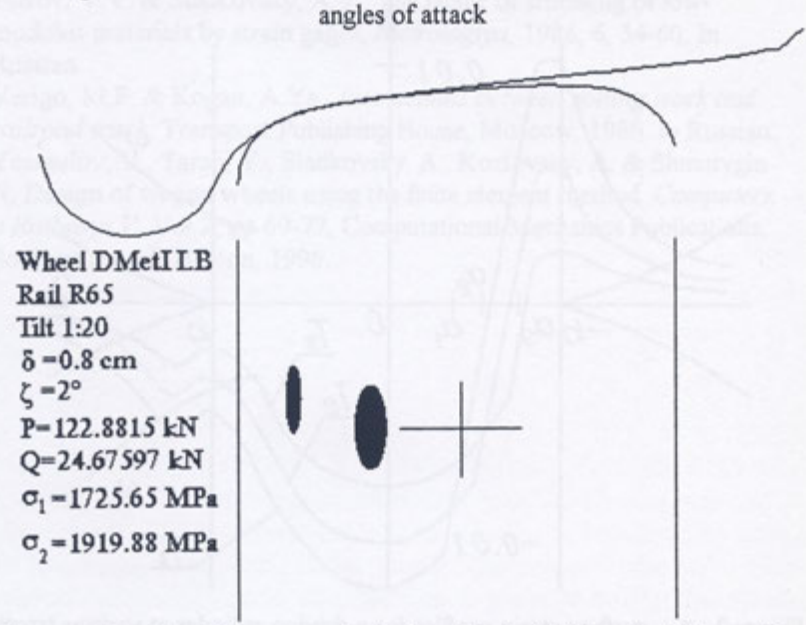

Figure 4: Results of computer simulation of wheel/rail contact inter-action. Wheel DMetI LB, rail R65, tilt of rail = 1:20, δ=0.8 cm, ζ=2°, P=122.8815 kN, Q=24.67597 kN, σ_1=1725.65 MPa, σ_2=1919.88 MPa